**Savunma Bilimleri Dergisi, 21(2): 267-290 (2025)**

SAVUNMA BİLİMLERİ DERGİSİ
*The Journal of Defense Sciences*

https://dergipark.org.tr/tr/pub/khosbd

# Ballistic Performance Analysis of Silicon Carbide Ceramic Body Armor Using Finite Element Method and Machine Learning Algorithms

## *Sonlu Elemanlar Yöntemi ve Makine Öğrenme Algoritmaları Kullanılarak Silisyum Karbür Seramik Vücut Zırhının Balistik Performans Analizi*

Halil Burak MUTU [1*]

[1]*Tokat Gaziosmanpaşa University, Faculty of Engineering And Architecture, Department of Mechanical Engineering, Tokat, Türkiye*

**Makale Bilgisi**

*Araştırma makalesi*
*Başvuru: 30.06.2025*
*Düzeltme: 29.08.2025*
*Kabul: 09.09.2025*

**Keywords**

*Ballistic*
*Silicon carbide*
*Body armor*
*Machine learning*
*Simulation*

**Anahtar Kelimeler**

*Balistik*
*Silisyum karbür*
*Vücut zırhı*
*Makine öğrenmesi*
*Simülasyon*

***Highlights***

*Experimental methods used to determine the ballistic properties of body armors are costly, time-consuming, and difficult to repeat for each parameter combination. In contrast, numerical methods and machine learning-based models provide the opportunity to analyze a large number of variables such as different bullet types, velocities, armor thicknesses, and material properties quickly and cost-effectively. In this article, finite element analysis and three different machine learning algorithms are used to determine the ballistic properties of ceramic body armors.*

***Graphical Abstract***

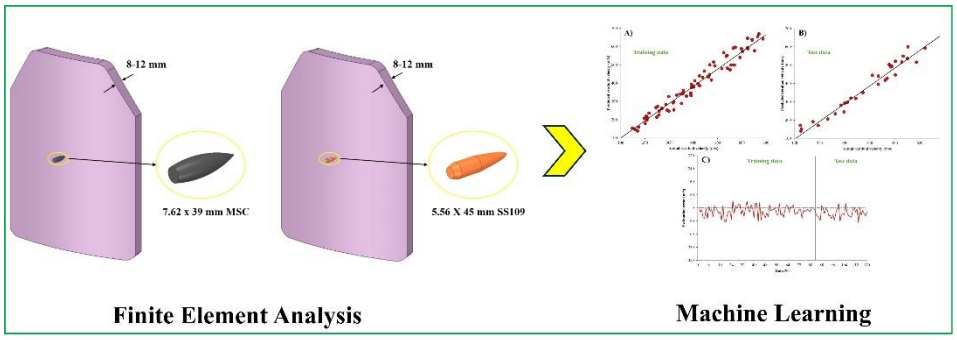


***Abstract***

*This study presents a machine learning-based approach for predicting the residual velocity of projectiles impacting silicon carbide (SiC) ceramic body armor plates of varying thicknesses. Explicit dynamic simulations were performed using the ANSYS finite element software to model the ballistic response of the armor under high-velocity impact. Simulation data were used to train and evaluate three different machine learning models: Linear Regression, ElasticNet, and Multilayer Perceptron (MLP). The predictive performance of each model was assessed using the coefficient of determination (R), mean absolute error (MAE), and root mean square error (RMSE) metrics across both training and testing datasets. Among the tested algorithms, the MLP model achieved the highest accuracy and lowest error values, demonstrating superior capability in capturing the complex nonlinear relationships governing ballistic impact phenomena.*

***Özet***

*Bu çalışma, farklı kalınlıklardaki silisyum karbür (SiC) seramik vücut zırh plakalarına çarpan mermilerin artık hızını tahmin etmek için makine öğrenmesine dayalı bir yaklaşım sunmaktadır. Zırhın yüksek hızlı darbe altındaki balistik tepkisini modellemek için ANSYS sonlu elemanlar yazılımı kullanılarak açık dinamik simülasyonlar gerçekleştirilmiştir. Simülasyon verileri, üç farklı makine öğrenimi modelini eğitmek ve değerlendirmek için kullanıldı: Doğrusal Regresyon, ElasticNet ve Çok Katmanlı Algılayıcı (MLP). Her modelin öngörü performansı, hem eğitim hem de test veri kümelerinde belirleme katsayısı (R), ortalama mutlak hata (MAE) ve kök ortalama kare hata (RMSE) metrikleri kullanılarak değerlendirildi. Test edilen algoritmalar arasında MLP modeli en yüksek doğruluk ve en düşük hata değerlerine ulaşarak, balistik çarpma olaylarını yöneten karmaşık doğrusal olmayan ilişkileri yakalamada üstün bir yetenek sergiledi.*

*Corresponding author, e-mail: halilburak.mutu@gop.edu.tr

DOI: 10.17134/khosbd.1731217

Elektronik/Online ISSN: 2148-1776
Basılı/Printed ISSN: 1303-6831

## 1. INTRODUCTION

For military and law enforcement personnel, body armor is a critical piece of equipment that increases the chance of survival in combat environments. With its first examples dating back to 2600 BC, armor has evolved from heavy metal parts to lightweight ceramic and composite systems with technological advances. Today's armor is manufactured within the framework of various standards in accordance with its intended use, aiming for an optimum balance between durability and mobility. In this context, ballistic material research continues. Body armor has been an indispensable part of personal defense throughout history. As is the case today, armor, which has been one of the important protective systems that increased people's chances of survival in the past, has evolved according to constantly changing war technologies and ammunition types. Armor systems have diversified with the development of material technology. Plate armor has become widespread in medieval Europe since the 14th century. These armors, which are made by combining leather and metal, were manufactured from iron, especially in Italy in the 15th century. However, with the increasing effectiveness of firearms on the battlefield, these armors became insufficient, and thicker and heavier armors were developed. Armors, which weighed approximately 15 kg in the 14th and 15th centuries, increased to 25 kg by the end of the 16th century [1]. This significantly limited the mobility of soldiers. As of the 20th century, the development of ammunition and weapons created the need for more effective protection systems. At this point, metal armors were replaced by lightweight, flexible, energy-absorbing materials. Modern body armors are manufactured especially from ceramic and fiber-reinforced composite materials. These materials provide both lightness and durability thanks to their low density and high hardness. The idea of using ceramic materials as armor dates back to the 20th century. It emerged towards the end of World War II and was first effectively applied during the Vietnam War. Today, armor systems are manufactured according to different ballistic standards worldwide. Various ceramic and composite combinations are preferred depending on the purpose of use and threat level. With the development of technology, research on new generation materials that can be used in the ballistic field continues. After the long-term dominance of steel, steel plates have been replaced by more advanced structural systems with the development of armor-piercing ammunition. This process has made it necessary to both lighten and make armor more effective in order to increase mobility. Thus, advanced ceramics have begun to be widely used in ballistic armor.

Advanced ceramics are high-performance materials consisting of crystal structures with high purity and controlled composition. They are subject to much more precise production processes compared to traditional ceramics; this makes them superior in terms of both structural strength and functional performance. The desired mechanical, thermal, and ballistic properties can be achieved by carefully adjusting the raw material ratios used during production. Such ceramics are generally produced from high-quality and finely ground powders [2]. Various molding methods, such as dry pressing, isostatic

pressing, and wet forming, are used in the production of advanced ceramics. In some cases, additional processes may be required after sintering to gain the final properties. Thanks to these processes, the crystal structure is made denser, smoother, and more impact-resistant. Advanced ceramics are among the ideal materials in ballistic applications due to their light weight and high hardness/strength ratios [3-5]. The primary purpose of the armor system is to stop the bullet coming at high speed and prevent it from contacting the human body. In this context, ceramics perform better than traditional metal armor because they can provide the same level of protection with much lower density.

Today, advanced ceramics such as aluminum oxide, boron carbide, silicon carbide, zirconia-reinforced alumina, and silicon nitride are widely used in armor systems. Among these, SiC is one of the prominent materials in ballistic armors. SiC, with its properties such as low density, high hardness, and excellent thermal conductivity, is the primary ceramic material preferred in both personal armor systems and military vehicles. Being lighter than aluminum oxide and more economical than boron carbide makes it ideal in terms of cost-performance [6]. In addition, SiC's high melting point and ability to limit microcrack propagation after impact increase its resistance to multiple impacts. In this respect, its resistance, especially against steel-core ammunition, is higher than that of other ceramics such as alumina and boron carbide. Although brittleness is a general disadvantage of advanced ceramics, SiC offers a more balanced performance in this respect.

In the literature, researchers have conducted experimental and numerical studies on the ballistic properties of ceramic armors. Cui et al. [7] conducted a comprehensive analysis of the ballistic performance of monolithic ceramics, including alumina, silicon carbide, boron carbide, and titanium diboride ($TiB_2$), based on existing literature data. The study examined various calibers and projectile velocities ranging from 500 to 2700 m/s. The influence of different ceramic types and their properties on depth of penetration (DOP), excluding ceramic thickness, and the differential efficiency factor (DEF), was systematically investigated. The findings demonstrated that projectile velocity, ceramic material, and tile thickness significantly affect ballistic performance. DEF correlated with the ceramic density, with boron carbide, silicon carbide, alumina, and titanium diboride exhibiting the highest efficiency. Additionally, DEF increased with ceramic thickness, which was consistent with the observed trends in DOP. Both DOP and DEF initially increased with projectile velocity but decreased at higher speeds. The DEF parameter accounts for penetration into the backing plate, which increases with velocity and consequently reduces DEF. Ceramic thickness also affects residual penetration, showing a linear relationship between penetration depth and thickness. However, as thickness and density increase, DEF tends to decrease if there is no corresponding reduction in DOP, reflecting the balance between protection and mass efficiency. Optimal ballistic efficiency against armor-piercing projectiles was observed at impact velocities between 800 and 900 m/s. Furthermore, a correlation between flexural

strength and ballistic performance suggests that flexural strength could serve as a useful evaluation criterion for ceramic armor materials.

Savio et al. [8] investigated the influence of backing materials, projectile velocity, and ceramic tile thickness (alumina, boron carbide, and zirconia toughened alumina—ZTA) on ballistic performance against 7.62 × 54 mm armor-piercing projectiles through depth of penetration (DOP) testing. Experiments were conducted at velocities ranging from 600 m/s to 820 m/s. The study introduced a novel ballistic efficiency metric, the normalized differential efficiency factor (NDEF), which normalizes the thickness efficiency of DEF to exclude the effect of backing material resistance. Additionally, the normalized ballistic efficiency (NBE) was proposed, eliminating the influence of backing material density. Both NDEF and NBE exhibited a clear trend: ballistic efficiency of the ceramics decreased with increasing projectile velocity. Moreover, NBE and NDEF showed comparable trends regarding ceramic thickness and projectile velocity. Consequently, NBE was identified as the most effective parameter for evaluating ballistic efficiency and classifying ceramic materials, as it effectively removes the impact of backing material resistance and density from the efficiency assessment.

Hu et al. [9] investigated the ballistic behavior of silicon carbide mosaic tiles with varying geometries, combined with an ultra-high molecular weight polyethylene (UHMWPE) backing layer, under impact from 7.62 x 51 mm armor-piercing projectiles at velocities around 780 m/s. Their findings demonstrated that the mosaic configuration extends the interaction time between the projectile and the target, resulting in erosion and deceleration of the projectile within the ceramic front layer, while the residual kinetic energy is absorbed by the backing material. Moreover, ceramic properties such as hardness, fracture toughness, and flexural strength were identified as critical factors influencing ballistic performance.

Shen et al. [10] conducted experimental tests on silicon carbide mosaics backed by UHMWPE, incorporating bonding adhesives between the layers. These tests were performed near the ballistic limit using 7.62 mm steel-core projectiles with initial velocities ranging from 776 m/s to 791 m/s. They developed a numerical model employing design point and Monte Carlo methods to analyze dynamic responses and assess armor reliability. Results revealed that adhesive strength significantly enhances ballistic performance by mitigating bulging deformation in the backing layer.

Experimental and numerical methods have traditionally been used to analyze ballistic properties of armor. However, these approaches are often time-consuming and computationally expensive, with limited availability of comprehensive experimental databases. Recently, hybrid techniques combining numerical simulations with machine learning (ML) have emerged, enabling rapid analysis and extensive data generation. ML algorithms are increasingly applied in ballistic armor design for material selection, impact resistance evaluation, structural optimization, and dynamic impact analysis. These data-driven methods enhance armor performance while reducing costs by accurately predicting armor deformation under

varying conditions, thus minimizing the need for extensive physical testing. Additionally, AI-assisted finite element analysis (FEA) contributes to the development of lightweight and high-strength armor systems, promoting design innovation and efficiency. Overall, integrating machine learning into ballistic protection research improves protective capabilities and streamlines manufacturing processes.

Ryan et al. [11] employed machine learning regression models—including Extreme Gradient Boosting (XGBoost), Artificial Neural Networks (ANN), Support Vector Regression (SVR), and Gaussian Process Regression (GP)—to predict the ballistic limit of metallic armor against small and medium caliber projectiles, as well as the penetration depth into semi-infinite targets. Artero-Guerrero et al. [12] utilized an ANN to predict laminate deformation around the ballistic limit and identify optimal laminate configurations. Their approach integrated experimental results with finite element simulations to develop the ANN training dataset.

Wang and Sun [13] investigated the ballistic behavior of hybrid aramid fiber reinforced plastic (AFRP)/carbon fiber reinforced plastic (CFRP) laminates by integrating numerical simulations and machine learning. Finite element analyses were conducted in ABAQUS, modeling bullet impacts at 30°, 60°, and 90°, with velocities ranging from 300 to 900 m/s in 50 m/s increments. Residual projectile velocities were predicted in real-time using ANN and decision tree regression (DTR) models trained on ballistic data. Both models demonstrated strong predictive accuracy on experimental datasets, which improved further when trained on larger datasets generated from finite element simulations, highlighting the efficacy of combining data-driven and numerical methods for ballistic impact prediction. Khan et al. [14] investigated the prediction of penetration depth (PD) in ultra-high-performance concrete (UHPC) targets under ballistic impact by integrating interpretable ML approaches with deep generative adversarial network (DGAN)-based data augmentation. Using 103 experimental data points from the literature, a synthetic dataset of 10,000 entries was generated via DGAN, which successfully replicated the statistical characteristics of the real data. Five ML algorithms—decision tree (DT), XGBoost, random forest (RF), CatBoost, and LightGBM—were trained using projectile parameters (impact energy, velocity, diameter, mass) and UHPC properties (compressive strength, fiber addition) as inputs. The XGBoost model achieved the highest accuracy, with R = 0.990 and MAE = 4.933 for both training and testing sets. Comparative analysis showed that ML models outperformed empirical penetration models, highlighting their superior predictive capability. Model interpretability was enhanced using SHapley Additive exPlanations (SHAP), individual conditional expectation (ICE), and partial dependence plots (PDP), which revealed that projectile features were the dominant PD-influencing factors, followed by UHPC compressive strength and fiber content. The study demonstrated that combining interpretable ML with DGAN is an effective strategy for accurate PD estimation in UHPC with limited datasets, offering potential for reducing experimental requirements. Limitations include the omission of parameters such as aggregate size and type,

which have been shown to affect PD. Future work could explore hybrid ML models, alternative data augmentation techniques, and the development of ML-derived empirical equations for UHPC ballistic performance prediction.

Zhu et al. [15] developed a hybrid machine learning framework to predict the ballistic performance of multilayer composite armor against high-velocity projectiles. The study addressed the challenge of balancing lightweight structures with robust protection by combining Support Vector Machine (SVM) and Deep Neural Network (DNN) models, with hyperparameter optimization enhancing predictive accuracy. The framework was validated using a numerical computational model simulating the dynamic response of composite armor, comprising steel front and rear panels with a ceramic and fiber-reinforced composite core, and was benchmarked against experimental data on ballistic limit velocity and damage morphology. The SVM model accurately predicted armor penetration, with the radial basis function (RBF) kernel showing the best performance after optimization, while the DNN model predicted residual projectile kinetic energy and rear panel deformation with high precision. The hybrid framework, trained on 302 high-fidelity numerical samples, enables rapid and near real-time predictions of armor damage states, significantly reducing computational time from 96 core hours to under 10 seconds. This approach demonstrates the potential of integrating data-driven ML techniques for efficient and reliable prediction of multilayer composite armor performance under extreme impact conditions, providing a foundation for constructing a comprehensive "damage database" to support engineering design and operational decision-making. Mutu et al. [16] numerically investigated the ballistic performance of multilayered armor systems composed of alumina ceramic front layers supported by Kevlar-29 and ultra-high molecular weight polyethylene (UHMWPE) composites in various thickness ratios, maintaining a total composite layer thickness of 10 mm. Using LS-DYNA, they conducted 735 simulations with 7.62 mm armor-piercing projectiles at velocities between 700–1000 m/s (50 m/s increments) and three different failure strain (FS) erosion criteria on 35 armor configurations. The simulation results—validated against literature data—were used to train MLP, SVM, and DT machine learning models to predict residual projectile velocities based on ceramic thickness, composite configuration, projectile velocity, FS, and material properties. The findings revealed that increasing ceramic thickness reduced residual velocity, and higher UHMWPE content in the composite layers enhanced ballistic resistance. Among the tested algorithms, SVM achieved the highest prediction accuracy, with MAE values of 1.8826 (training) and 6.6731 (testing), and RMSE values of 3.4102 and 9.0483, respectively, accurately estimating approximately 82 % of residual velocities with an absolute error below 6 m/s. The study demonstrated that ML approaches can effectively complement traditional engineering methods in early-stage armor design, enabling efficient configuration screening, material selection, and performance prediction, thereby reducing the need for costly and time-consuming physical tests while fostering innovative design strategies in

defense applications. Lei et al. [17] developed an ML model to predict the ballistic impact performance of unidirectional fiber-reinforced composite plates (UD-FRCP) by linking macroscopic energy absorption to microstructural characteristics, quantified via the two-point correlation function. Using 185 micro-scale simulation cases for training, the proposed model achieved an average prediction error of 6.94% and a maximum error of 12.69%, demonstrating both high accuracy and computational efficiency. Critical parameter sensitivities were analyzed, showing that increasing the number of estimators in gradient boosting regression (GBR) and random forest regression (RFR) improved accuracy up to a saturation point, while decision-tree-based algorithms, particularly GBR, provided the best predictive performance. The study also highlighted the effect of training dataset size, confirming that 185 cases were sufficient for reliable predictions without excessive computational cost. Lei et al. [13] concluded that their ML approach effectively models the relationship between microstructure and impact protective performance, providing a rapid and accurate method for designing UD-FRCP with optimized ballistic resistance, and suggested extending the method to various fiber types, matrix materials, and microstructural topologies in future research. Kazarinov and Khvorov [18] explored the use of ANN to accelerate the numerical evaluation of residual impactor velocities for perforated PMMA targets, addressing the computational challenges of high-fidelity finite element method (FEM) simulations. The ANN models were trained on FEM-generated datasets incorporating the incubation time fracture criterion, enabling rapid predictions of impact strength for target configurations without requiring computationally intensive FEM runs. The study demonstrated that fully connected ANNs outperformed convolutional architectures for predicting static plate deflection, while convolutional networks were effective for dynamic impact problems. Moreover, the ANN models were capable of extrapolating to configurations that caused FEM failures due to extreme mesh distortions, achieving high prediction accuracy ($R^2 = 0.961$) for problematic cases. By integrating the ANN with a genetic algorithm, optimized perforation patterns were generated that theoretically enhanced impact resistance by distributing spall-related fractures and reducing residual projectile velocities. The approach significantly reduced computational time, bypassed FEM instabilities, and allowed fast evaluation of design variants, providing a robust tool for both prediction and optimization of perforated plate impact performance. The study highlighted the potential of ANN-assisted frameworks to complement FEM in complex impact problems and streamline design processes.

Although various studies have analyzed the ballistic performance of ceramic armors using experimental methods or finite element simulations, applications that combine such simulations with ML for predictive modeling remain limited. In particular, there is a lack of research focusing on SiC body armors subjected to impacts from multiple types of rifle projectiles, such as both 7.62 x 39 mm Mild Steel Core (MSC) and 5.56 x 45 mm SS109 bullets, within the same study. Existing ML-based ballistic

prediction works often employ small datasets and consider only a narrow range of parameters, typically limited to a single projectile type or basic impact velocity. Furthermore, comparative evaluations of different ML algorithms for this specific application are scarce, especially using large datasets generated from high-fidelity finite element models.

In this study, the ballistic properties of SiC body armors with different thicknesses against high-velocity 7.62 x 39 mm MSC and 5.56 x 45 mm SS109 bullets were investigated by the finite element method. As a result of the analyses, a data set was created for the residual velocities depending on the bullet type, bullet muzzle velocity, ceramic thickness, and mesh size. The obtained data were used to train the LinearRegression, ElasticNet, and MLP algorithms; thus, the aim was to estimate the residual velocity values after the bullet impact. A total of 600 data points were generated for each data set in the ML algorithms. 70% of the data set was used for training, while 30% was used for testing. The prediction results of the LinearRegression, ElasticNet, and MLP machine learning algorithms were evaluated according to three performance criteria.

## 2. MATERIAL AND METHODS

### 2.1. Finite Element Analysis

7.62 x 39 mm MSC, 5.56 x 45 mm SS109, and SiC body armors of different thicknesses were modeled with the Ansys/SpaceClaim module. In the analyses, body armors of 8, 9, 10, 11, and 12 mm thicknesses were used in accordance with the measurements of ceramic body armors produced for ballistic protection today. The steel cores of the 7.62 x 39 mm MSC and 5.56 x 45 mm SS109 bullets were positioned to contact the armor. Finite element models of the bullets and armors are given in Figure 1.

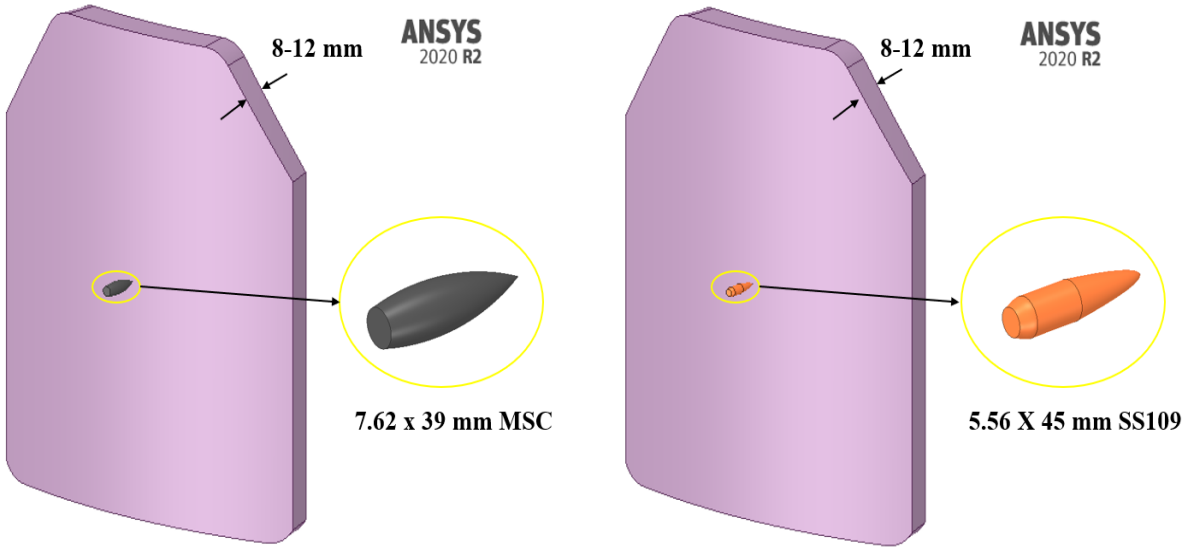


**Figure 1:** Ballistic body armor and bullets.

7.62 x 39 mm MSC is an infantry rifle ammunition developed by the Soviets and generally used in weapons such as the AK-47 and SKS. 5.56 x 45mm SS109 is an ammunition developed to NATO standards and used in the M16 and its derivatives. These two bullets were preferred in numerical analyses. A summary of the nominal data of the bullets is given in Table

1. The technical drawing of the ammunition is shown in Figure 2.

**Table 1:** Summary of the nominal data of the bullets.

| Ammunition | Gun | Bullet mass (g) | Expected Muzzle Velocity [m/s] |
|---|---|---|---|
| 7.62x39 mm MSC | AK-47, SKS | 8 (123 grain) | ~715 m/s |
| 5.56x45mm SS109 | M16, M4 | 4 (62 grain) | ~920 m/s |

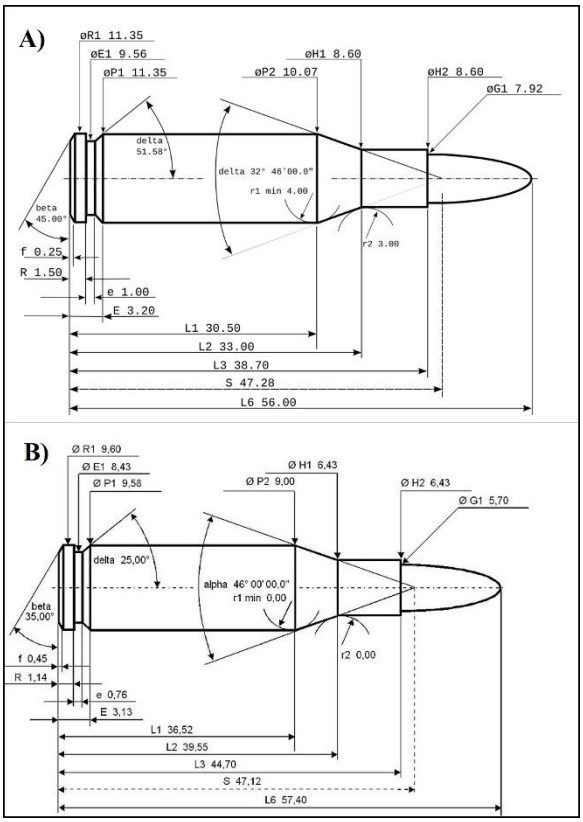


**Figure 2:** Ammunition technical drawings A) 7.62x39 mm MSC cartridge B) 5.56x45mm SS109 cartridge [19].

Finite element analyses of ceramic armors were performed with the Ansys/Explicit Dynamics module. Two different mesh structures were used in the analyses. Mesh structures are shown in Figure 3.

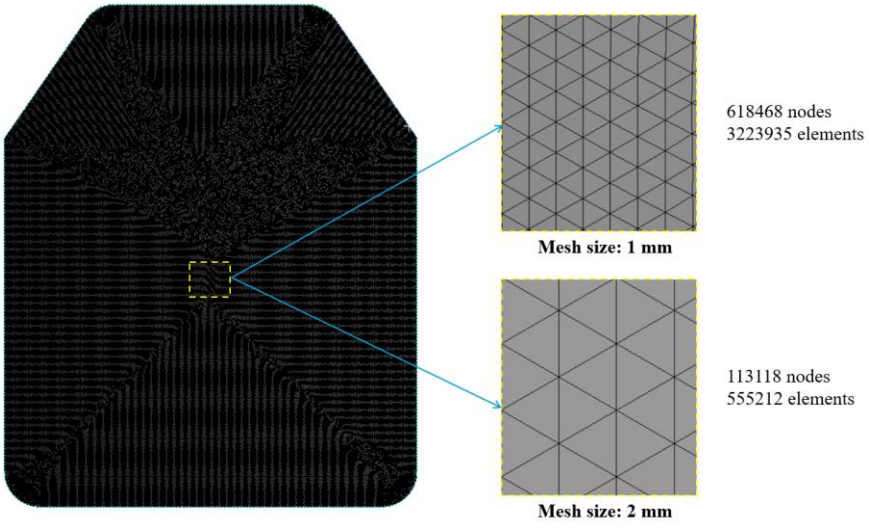


**Figure 3:** Mesh structures of body armor.

In the analysis, 7.62x39 mm MSC bullet hit targets consisting of SiC ceramics with 5 different thicknesses with speeds between 750 m/s and 1000 m/s; 5.56x45 mm SS109 bullet hit targets consisting of 5 different thicknesses with speeds between 950 m/s and 1200 m/s. The changed parameters and values are given in Table 2.

**Table 2:** Parameters and values used in the analysis.

| Parameter | Bullet type | Bullet muzzle velocity (m/s) | Ceramic thickness (mm) | Mesh size (mm) |
|---|---|---|---|---|
| | | 750 | 8 | |
| | | 800 | 9 | |
| | 7.62x39 | 850 | 10 | 0.5 |
| | mm MSC | 900 | 11 | 1 |
| | | 950 | 12 | |
| | | 1000 | | |
| **Value** | | | | |
| | | 950 | 8 | |
| | | 1000 | 9 | |
| | 5.56x45mm | 1050 | 10 | 0.5 |
| | SS109 | 1100 | 11 | 1 |
| | | 1150 | 12 | |
| | | 1200 | | |

The Johnson Cook material chart is used to describe the behavior of the steel core of the bullet in the finite element method. In this model, the equivalent stress is:

$$\sigma_y = \left[A + B\varepsilon_p^n\right]\left[1 + C\ln\left(\frac{\varepsilon}{\varepsilon_0}\right)\right]\left[1 - \left(\frac{T-T_r}{T_{melt}-T_r}\right)^M\right] \quad (1)$$

$\sigma_y$ symbolize the yield stress of the material, $\varepsilon_p$ represents the equivalent plastic deformation, $\varepsilon/\varepsilon_0$ represents the dimensionless deformation ratio; A, B, C, M, and n represent the material constants. T, $T_r$, and $T_{melt}$ represent the current, room, and melting temperatures, respectively. The material properties of the Steel 4340 steel bullet core used in the analysis are given in Table 3.

**Table 3:** Johnson-Cook material parameters for bullet [20].

| Parameter | Symbol | Value | Unit |
|---|---|---|---|
| **Linear EOS, Johnson– Cook strength, failure** | | | |
| Density | ρ | 7.83 | g/cm$^3$ |
| Shear modulus | G | 7.7 x 10$^7$ | kPa |
| Strain hardening constant | B | 5.1 x 10$^5$ | kPa |
| Strain rate constant | C | 0.014 | - |
| Melting temperature | $T_m$ | 1793 | °K |
| Room temperature | $T_r$ | 300 | °K |
| Bulk modulus | - | 1.59 x 10$^8$ | |
| Yield strength | A | 7.92 x 10$^5$ | kPa |
| Strain hardening exponent | n | 0.26 | |
| Thermal softening exponent | m | 1.03 | |
| Reference strain rate | ε | 1 | s$^{-1}$ |
| Damage constant | $D_1$ | 0.05 | - |
| Damage constant | $D_2$ | 3.44 | - |
| Damage constant | $D_3$ | 0.61 | - |
| Damage constant | $D_4$ | -2.12 | - |
| Damage constant | $D_5$ | 0.003 | - |

Explicit Dynamics is a nonlinear analysis software widely employed for the simulation of complex physical phenomena, including impact, penetration, explosions, and blast events [21]. The program incorporates a broad range of advanced material constitutive models to represent material behavior under extreme conditions accurately. Among these, the Johnson–Holmquist-1 (JH-1) model—characterized by its linear segmented approach to material strength and failure—has been integrated into Explicit Dynamics to enhance its

capabilities in advanced material modeling further.

Users of Explicit Dynamics can choose between two modeling approaches when defining the Johnson–Holmquist material behavior: the "Segmented" (JH-1) or the "Continuous" (JH-2) type. When the segmented JH-1 model is selected for strength, it must also be used for the failure model; in other words, the segmented strength model cannot be combined with the continuous failure model. Conversely, both segmented (JH-1) and continuous (JH-2) failure models are compatible with the continuous (JH-2) strength model. Validated material property data for SiC using the JH-1 model are presented in Table 4 and are included in the standard material library of Explicit Dynamics version 2020 R2 [20].

**Table 4:** Johnson-Holmquist material parameters for SiC [22].

| Parameter | Symbol | Value | Unit |
|---|---|---|---|
| **Equation of state: polynomial** | | | |
| Density | ρ | 3.215 | g/cm$^3$ |
| Bulk modulus | $A_1$ | 2.20 x 10$^8$ | kPa |
| Parameter | $A_2$ | 3.61 x 10$^8$ | kPa |
| Parameter | $T_1$ | 2.20 x 10$^8$ | kPa |
| **Strength: Johnson–Holmquist, segmented** | | | |
| Shear modulus | G | 1.93 x 10$^8$ | kPa |
| Hugoniot elastic limit | HEL | 1.17 x 10$^7$ | kPa |
| Intact strength constant | $S_1$ | 7.10 x 10$^6$ | kPa |
| Intact strength constant | $P_1$ | 2.50 x 10$^6$ | kPa |
| Intact strength constant | $S_2$ | 1.22 x 10$^7$ | kPa |
| Intact strength constant | $P_2$ | 1 x 10$^7$ | kPa |
| Strain rate constant | C | 0.009 | - |
| Max. fracture strength | $S_{max}$ | 1.30 x 10$^6$ | kPa |
| Failed strength constant | α | 0.4 | - |
| **Failure: Johnson–Holmquist, segmented** | | | |
| Hydro tensile limit | T | -7.50x 10$^5$ | kPa |
| Damage constant | $\varepsilon_{max}$ | 0.8 | - |
| Damage constant | $P_3$ | 9.975x 10$^7$ | kPa |
| Bulking constant | β | 1 | - |

## 2.2. Model Validation

In order to evaluate the accuracy of the finite element model developed in this study, an experimental study conducted by Araslı [23] was taken as a reference. In that study, ballistic tests were performed on 12 mm thick SiC ceramic armor using a 7.62 mm caliber bullet, in accordance with the NIJ 0101.06 Level III ballistic protection standard. The experimental results indicated that a bullet impacting at a velocity of 833.04 m/s exhibited partial penetration, confirming the protective capability of the ceramic plate. These data were compared with the finite element analysis results obtained in the current study. A total of 8 representative test cases, covering different projectile types, impact velocities, and armor thicknesses, were used for validation. Additionally, the simulation results were benchmarked against commercially available 12 mm SiC ceramic armor plates, which are designed to stop both 7.62×39 mm MSC and 5.56×45 mm SS109 projectiles.

## 2.3. Machine Learning

### 2.3.1. Linear regression

Linear regression is one of the fundamental methods used for modeling the relationship between a dependent variable and one or more independent variables [24]. The main objective of this technique is to find a linear function that best predicts the value of the target variable based on the observed inputs. It is widely used due to its simplicity, interpretability, and effectiveness in a variety of practical scenarios where the relationship among variables is approximately linear.

The standard form of the linear regression model can be expressed as:

$$\hat{y} = w_0 + w_1x_1 + w_2x_2 + \cdots + w_nx_n \quad (2)$$

where: $\hat{y}$ denotes the predicted value of the target variable, $x_1, x_2, \ldots x_n$ represent the input (independent) variables, $w_0$ is the intercept (bias term), $w_1, w_2, \ldots w_n$ are the regression coefficients to be estimated from the data.

**2.3.2. Elastic Net**

In the realm of high-dimensional statistical modeling, the Elastic Net (ENET) has emerged as a powerful extension of the Lasso (Least Absolute Shrinkage and Selection Operator) method, offering enhanced robustness in the presence of highly correlated predictors [25]. While the lasso effectively performs variable selection by applying an $\ell 1$ penalty, it tends to produce unstable solutions when predictors exhibit strong multicollinearity. To address this critical limitation, the ENET was introduced as a more stable alternative, particularly suitable for high-dimensional settings such as genomics or signal processing, where extreme correlations are common [26].

The ENET achieves this improvement by incorporating a convex combination of the $\ell_1$ penalty used in lasso and the $\ell_2$ penalty applied in ridge regression. This dual-penalty framework not only encourages sparsity in the model (as with lasso) but also promotes grouping effects and solution stability (as with ridge). The general form of the ENET estimator is given by:

$$\hat{\beta}(\text{enet}) = \left(1 + \frac{\lambda_2}{n}\right)\left\{\underset{\beta}{\arg\min} \|y - X\beta\|_2^2 + \lambda_2\|\beta\|_2^2 + \lambda_1\|\beta\|_1\right\} \quad (3)$$

To simplify tuning, the penalty parameters $\lambda_1$ and $\lambda_2$ are often reparameterized using a mixing parameter $\alpha \in [0, 1]$, defined as:

$$\alpha = \lambda_2/(\lambda_1 + \lambda_2) \quad (4)$$

Under this formulation, the ENET optimization problem can be equivalently expressed as:

$$\hat{\beta}(\text{enet2}) = \underset{\beta}{\arg\min} \|y - X\beta\|_2^2 \text{ , subject to } P_\alpha(\beta) = (1-\alpha)\|\beta\|_1 + \alpha\|\beta\|_2^2 \leq s \quad (5)$$

where $P_\alpha(\beta)$ denotes the elastic net penalty term, and $s$ is a scalar threshold controlling the total regularization.

This reparameterization highlights the flexibility of the elastic net. When $\alpha = 1$, the model reduces to ridge regression, applying full $\ell_2$ penalization; when $\alpha = 0$, it simplifies to the lasso, with only an $\ell_1$ penalty applied. Intermediate values of $\alpha$ allow the method to balance sparsity and stability, depending on the structure of the data.

A key advantage of the ENET is its ability to handle grouped variable selection effectively. The $\ell_1$ component continues to perform automatic variable elimination by shrinking some coefficients to exactly zero. Meanwhile, the $\ell_2$ component stabilizes the estimation paths and encourages the selection of correlated groups of variables by shrinking their coefficients toward each other. This so-called "grouping effect" enables ENET to select entire clusters of related predictors even when the group membership is unknown a priori.

This characteristic is particularly beneficial in situations where the number of predictors $p$ far exceeds the number of observations $n$, a common scenario in modern data-rich disciplines. Unlike lasso, which is limited to selecting at most nnn variables in such cases, the elastic net can select more than nnn variables due to the inclusion of the $\ell_2$ term.

Despite these strengths, it is important to note that the elastic net does not possess the oracle property, a theoretical guarantee that allows consistent identification of the true model under certain conditions. Therefore, while the ENET improves prediction accuracy and model interpretability in practice, it may not always perfectly recover the underlying data-generating mechanism.

In summary, the elastic net serves as a versatile and powerful tool for regularized regression analysis in high-dimensional contexts. Combining the strengths of both lasso and ridge regression addresses key limitations and provides a more robust framework for variable selection and predictive modeling in the presence of collinearity.

**2.3.3. MLP**

The MLP is a type of ANN designed to mimic the operational principles of the human nervous system [27]. This architectural framework creates a computational model that processes information and performs designated tasks through a network of interconnected artificial neurons. ANNs consist of numerous neurons working collaboratively, each contributing to the solution of specific problems by performing targeted computations on the input data [28]. The capability of these networks to tackle complex problems primarily arises from the dynamic interactions between neurons distributed across multiple layers within the system.

One of the key strengths of ANNs lies in their ability to learn effectively from both experimental observations and numerical datasets, enabling their widespread application across diverse fields [29]. Moreover, neural networks offer considerable advantages in terms of ease of design and implementation, attributable to their generally intuitive and straightforward structural organization [30]. It has also been noted that such networks demonstrate significant improvements in computational performance, especially when handling large-scale datasets, due to their inherent speed and efficiency [31].

Specifically, in the case of the MLP, a network composed of a single layer is constrained to learning only linear relationships. However, by employing multiple layers, the MLP architecture gains the ability to model complex nonlinear functions. This expansion considerably enhances the network's capacity to address intricate and multidimensional problems. The typical MLP structure includes an input layer, one or more hidden layers, and an output layer, each fulfilling distinct roles that collectively contribute to the network's overall function. The input layer receives raw data, which is then processed and transformed into increasingly abstract representations by the hidden layers. Finally, the output layer interprets the processed information to produce the final result.

Thanks to this layered configuration, MLPs serve as powerful and flexible models capable of adapting to a wide range of challenges by toggling between linear and nonlinear relationships as needed. Consequently, MLPs have been found to be extensively used in various domains, particularly in tasks such as classification, regression, and time series prediction [32]. Figure 4 provides a schematic illustration of the MLP architecture as applied to

the estimation of residual velocity, highlighting its layered composition and operational flow..

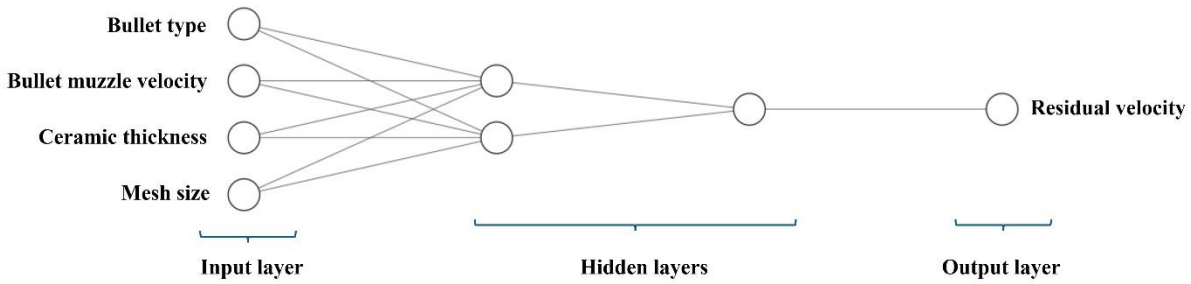


**Figure 4:** MLP architecture.

## 3. FINDINGS

In this study, the ballistic properties of SiC body armors with different thicknesses were analyzed using the finite element method with 7.62 x 39 mm MSC and 5.56 x 45 mm SS109 bullets. While the 7.62 x 39 mm MSC bullet hit the targets at speeds between 750 and 1000 m/s, the 5.56 x 45 mm SS109 bullet hit the target at speeds between 950 and 1200 m/s. The residual velocity values obtained from the analysis results were also estimated using machine learning algorithms.

### 3.1. Finite Element Analysis Results

As a result of the shots fired with both bullets, full penetration occurred in SiC body armors of all thicknesses due to high impact velocities. An increase in residual velocity values was observed depending on the bullet diameter and velocity. Figure 5 shows the deformations that occur as a result of a bullet impact on SiC body armor. Ceramic materials, widely used in armor systems due to their high hardness and compressive strength, exhibit complex fracture behavior when subjected to high-velocity ballistic impacts. A critical factor governing this behavior is deviatoric stress—the component of stress responsible for shape change (distortion) without a change in volume. Unlike hydrostatic stress, which primarily contributes to volumetric changes, deviatoric stress directly drives the initiation and propagation of fractures in brittle materials such as ceramics. Under ballistic impact conditions, deviatoric stress plays a dominant role in determining the onset of failure. As the intensity of deviatoric stress, particularly that arising from shear forces, increases, the rate and severity of fracture in ceramic materials also rise. This is especially significant given ceramics' inherent resistance to compressive loading. Once the deviatoric stress surpasses a critical threshold, localized shear deformation leads to crack initiation, ultimately resulting in catastrophic failure.

Fracture in ceramics occurs through a combination of mechanisms that are activated by the interaction of stress waves generated during impact. Initially, the high-velocity impact generates a compressive stress wave that propagates through the ceramic body. Upon reaching the free (unconfined) surface of the ceramic, part of this compressive wave reflects back as a tensile wave. The superposition of these stress fields—compressive and tensile—induces radial cracking that originates at the impact site and spreads outward. In addition to radial

fractures, circumferential (or hoop) cracks also develop due to bending moments induced along the radial direction. These bending stresses arise due to the differential deformation between the impacted zone and the surrounding material, leading to tensile stresses perpendicular to the radial cracks. This multi-modal cracking pattern, comprising both radial and circumferential fractures (Figure 5), is characteristic of brittle materials subjected to dynamic loading and plays a key role in energy dissipation and ballistic resistance. Similar cracking patterns have been documented in previous investigations of armor systems subjected to high-velocity projectile impacts [33-36].

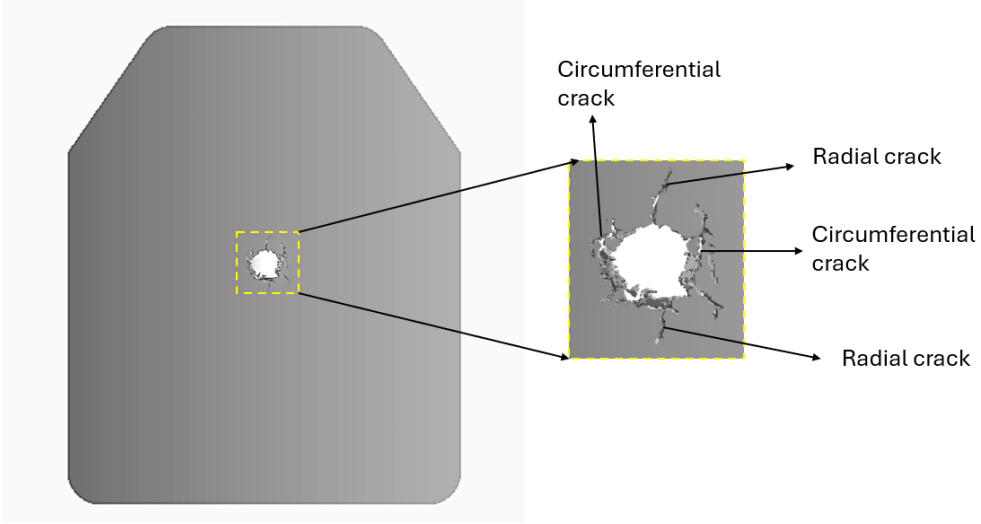


**Figure 5:** Fracture patterns in body armor.

In the field of ballistic engineering, certain specialized types of ammunition are deliberately designed to decelerate upon entering a target medium. This controlled reduction in velocity serves to disperse kinetic energy over a wider area, thereby maximizing the impact effect. Such ammunition typically incorporates a mechanism of controlled expansion—often referred to as “mushrooming”—upon contact with the target. This expansion significantly increases the diameter of the projectile, resulting in a larger wound channel and enhanced tissue disruption. The strategic design of these projectiles plays a critical role in applications where stopping power and internal damage are prioritized over penetration depth. Within the scope of the numerical analysis presented in Fig. 6, it is observed that the bullets undergoes substantial plastic deformation as a result of stress levels that significantly exceed the material's static yield strength of 792 MPa during its interaction with the target. This extreme deformation leads to a pronounced mushrooming effect in the bullet core, which is a critical indicator of energy transfer and material failure mechanisms under high-strain-rate conditions. The occurrence of such deformation is not merely a byproduct of the impact but is considered a key design feature, as it enhances the terminal ballistic performance of the projectile.

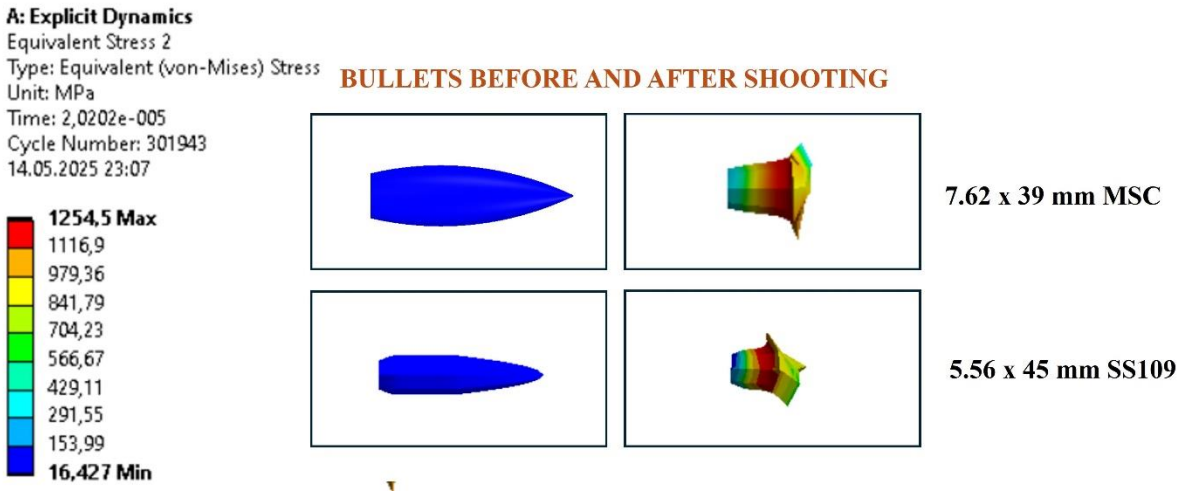


**Figure 6:** Deformation of bullets.

Crouch et al. [37] investigated the penetration behavior of AK47 MSC ammunition against boron carbide-based armor systems through experimental and numerical methods. In their study, the presence of relatively soft intermediate layers (the lead-filled jacket on the bullet and the fiber-reinforced polymer layer on the ceramic) between the steel core and the ceramic strike face was evaluated. Their findings revealed that the projectile core exhibited pronounced mushrooming on or near the ceramic surface, followed by a linear erosion process as it penetrated the ceramic. This two-stage deformation mechanism was associated with the projectile being subjected to stress levels exceeding the material's strength under high strain-rate loading. Similarly, in the present study, numerical analyses showed that the bullets experienced substantial plastic deformation under stresses significantly exceeding the static yield strength of 792 MPa, resulting in a pronounced mushrooming effect in the bullet core. In both studies, such deformation is emphasized not merely as a byproduct of impact, but as a key design feature that enhances the terminal ballistic performance of the projectile.

### 3.2. Machine Learning Result

The selection of Linear Regression, ElasticNet, and MLP algorithms for this study was based on their complementary capabilities in modeling complex relationships and their widespread use in predictive analytics. Linear Regression was chosen as a baseline model due to its simplicity, interpretability, and effectiveness in capturing linear relationships between input parameters and residual velocity. ElasticNet was selected to address potential multicollinearity among input features, as it combines the regularization benefits of both Lasso and Ridge regression, improving model generalization while maintaining interpretability. MLP, a type of feedforward neural network, was employed to capture the highly nonlinear and intricate interactions inherent in ballistic impact phenomena, which linear models may fail to represent accurately. By comparing these three methods, the study not only evaluates straightforward linear approaches but also demonstrates the superior predictive performance of MLP in complex, high-dimensional datasets.

As a result of ballistic analysis, three different performance metrics were included in this study to evaluate the performance of machine learning models in order to make more accurate velocity estimates. These metrics were determined as R, MAE, and RMSE.

The linear R shows how well the model's estimates match the real data, and as the R value approaches 1, the accuracy of the model's estimates increases. In other words, a high R indicates that the model provides more reliable results. MAE is another important criterion determining how close the predictions are to the actual values. A low MAE indicates that the model's prediction errors are minor, meaning that the model is more successful. RMSE is calculated by taking the square root of the average of the squares and comparing the differences between the model's predicted values and the actual values. A low RMSE indicates that the model's margin of error is smaller and, therefore, the predictions are more accurate.

When these three performance metrics are evaluated together, it is possible to analyze the prediction capabilities of machine learning models more objectively and comprehensively. Thus, the best-performing model can be selected, and the accuracy of ballistic analyses can be increased.

The formulations of the $R^2$, MAE, and RMSE statistical metrics for the prediction results of residual velocity are given in equations 6, 7, and 8.

$$R^2 = 1 - \frac{\sum^n (y-\hat{y})^2}{\sum^n (y-\bar{y})^2} \quad (6)$$

$$MAE = \frac{1}{n}\sum^n |y - \hat{y}| \quad (7)$$

$$RMSE = \sqrt{\frac{1}{n}\sum^n (y - \hat{y})^2} \quad (8)$$

In these equations, y represents the FEA data, $\hat{y}$ the predicted value, $\bar{y}$ the mean value of the FEA data, and n the number of samples in the dataset. Table 5 shows the training and test data of 3 different machine learning algorithms.

**Table 5:** Training and testing results of ML algorithms.

| Model No | ML Model | Training Set | | | Testing Set | | |
|---|---|---|---|---|---|---|---|
| | | R | MAE | RMSE | R | MAE | RMSE |
| 1 | LinearRegression | 0.5897 | 124.0397 | 143.3826 | 0.6311 | 136.4468 | 161.3921 |
| 2 | ElasticNet | 0.9289 | 52.7159 | 64.8966 | 0.9331 | 67.0142 | 81.8513 |
| 3 | MultilayerPerceptron | 0.9850 | 28.6245 | 36.1583 | 0.9884 | 36.6704 | 43.5008 |

Figure 7 presents the residual velocity estimation results for both the training and test sets using the LinearRegression method. From Figure 7, it is observed that the LinearRegression method achieved an R value of 0.5897, an MAE of 124.0397, and a RMSE of 143.3826 for the training set. For the test set, the LinearRegression method yielded an R value of 0.6311, an MAE of 136.4468, and an RMSE of 161.3921. Figure 7 also illustrates the residual velocity estimation errors obtained using the LinearRegression methods. The error values on the y-axis represent the difference between the predicted and FEA residual velocity values. The prediction errors for the LinearRegression technique is shown as orange lines in Figure 7(C) for both training and test sets. A larger deviation from the zero point on the y-axis indicates poorer prediction performance, while a smaller deviation indicates superior prediction accuracy.

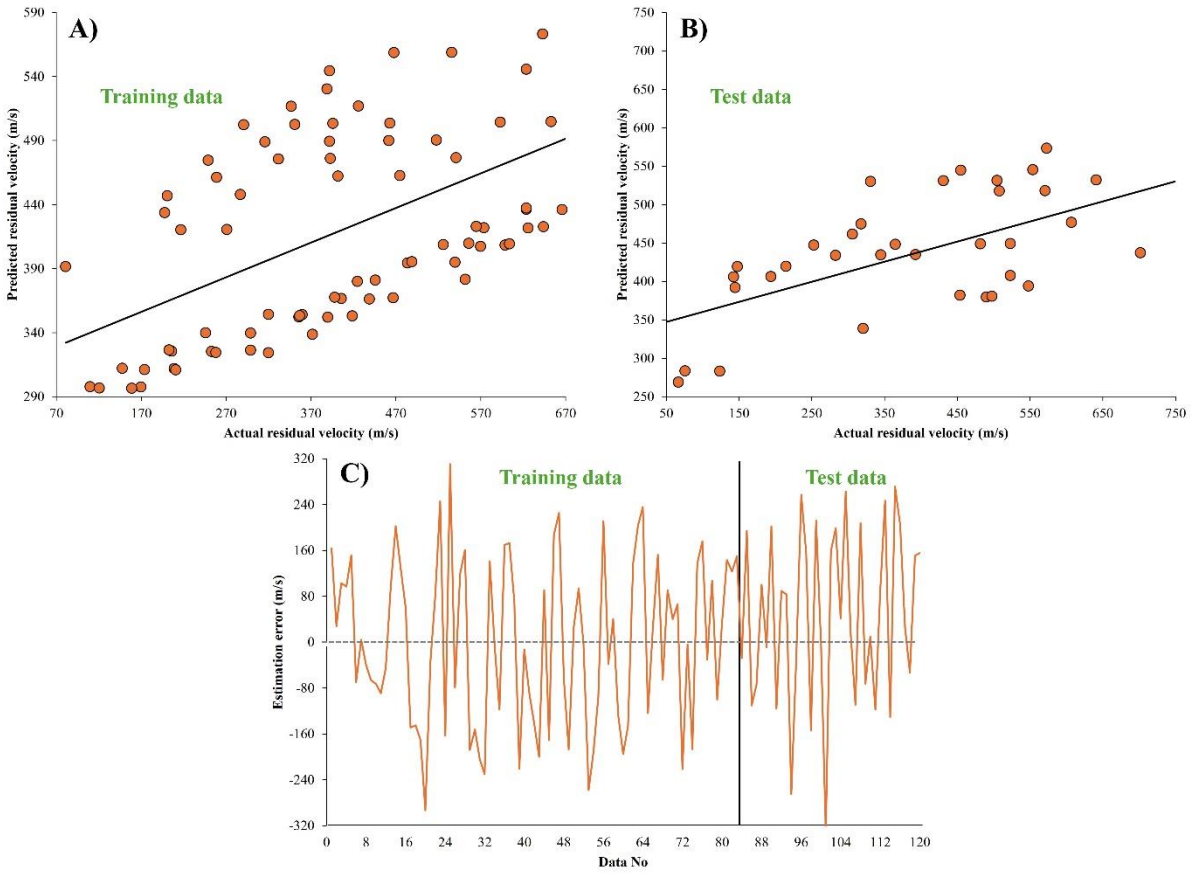


**Figure 7:** LinearRegression estimation results.

Figure 8 illustrates the residual velocity estimation outcomes for both the training and test datasets obtained via the ElasticNet algorithm. As shown, the ElasticNet method attained an R value of 0.9289, an MAE of 52.7159, and an RMSE of 64.8966 for the training data. In the test set, it yielded an R value of 0.9331, an MAE of 67.0142, and an RMSE of 81.8513. The figure further displays the residual velocity estimation errors derived from the LinearRegression approach. The y-axis denotes the discrepancy between the predicted and FEA-obtained residual velocities. In Figure 8(C), the prediction errors corresponding to the ElasticNet technique are depicted with purple lines for both datasets. A greater deviation from zero on the y-axis reflects reduced prediction performance, whereas a smaller deviation signifies higher predictive accuracy.

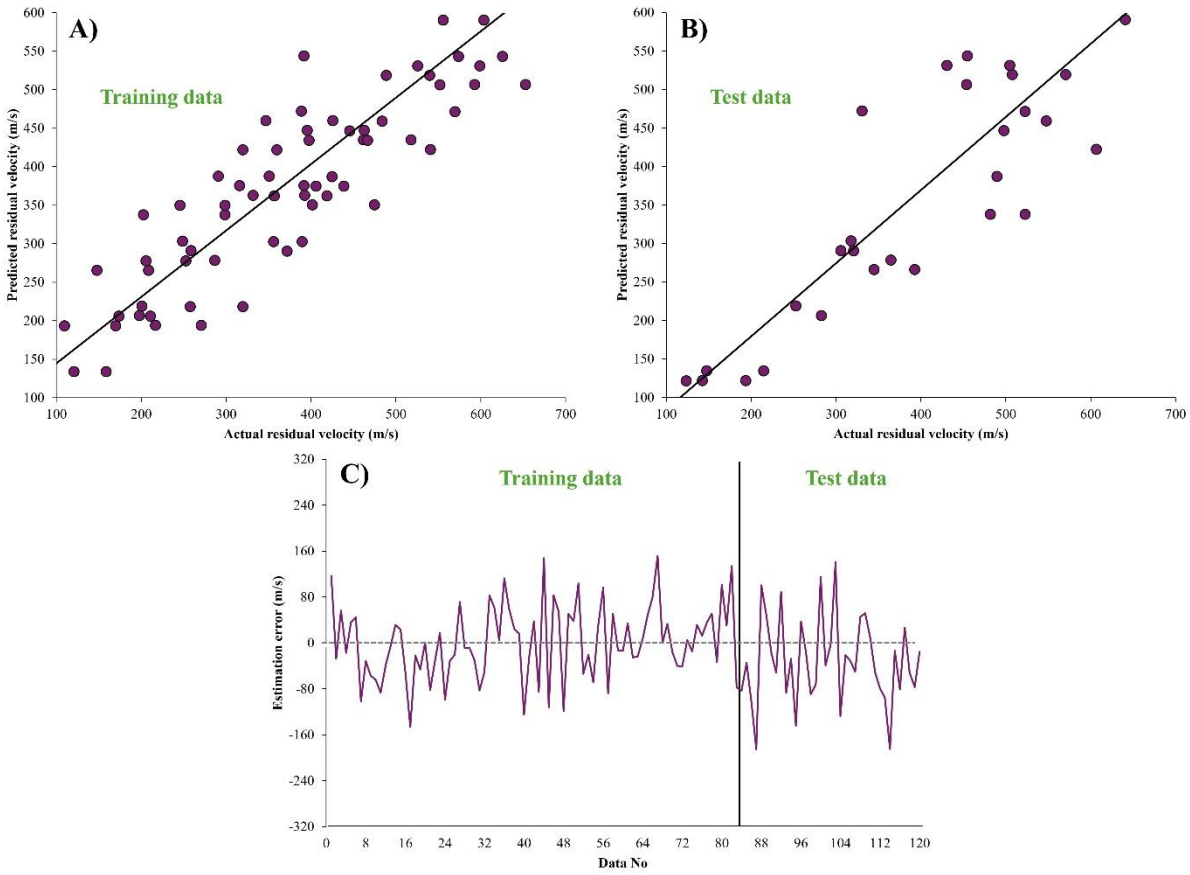


**Figure 8:** ElasticNet estimation results.

Figure 9 presents the residual velocity estimation results for both training and test datasets using the MLP method. As shown in Figure 9, the MLP approach achieved an R value of 0.9850, an MAE of 28.6245, and an RMSE of 36.1583 for the training set. For the test set, the LinearRegression method yielded an R value of 0.9884, an MAE of 36.6704, and an RMSE of 43.5008. Additionally, Figure 9 depicts the residual velocity estimation errors obtained via the MLP method. The error values on the y-axis indicate the difference between the predicted and FEA-based residual velocities. In Figure 9(C), the prediction errors associated with the MLP method are represented by red lines for both datasets. Greater deviations from zero on the y-axis reflect lower prediction performance, whereas smaller deviations correspond to higher estimation accuracy.

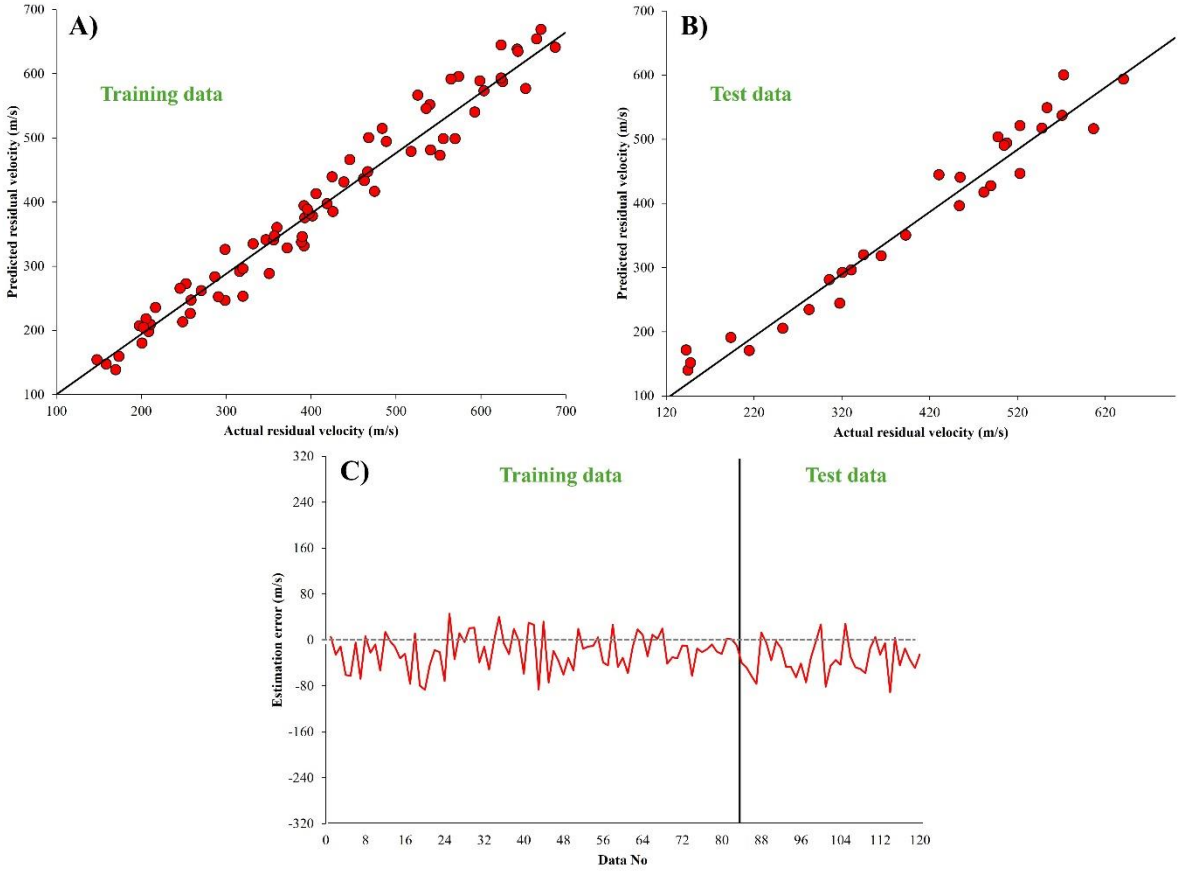


**Figure 9:** MLP estimation results.

**Table 6:** Generated equations with the linear regression and the elastic net algorithms.

| **Predicted parameter with linear regression** |
|---|
| Residual velocity = 204.5635 * Bullet type + 1.6878 * Bullet muzzle velocity + -71.9645 * Ceramic thickness + -1911.6902 |
| **Predicted parameter with elastic net** |
| Residual velocity = 7.691 * Bullet type + 0.554 * Bullet muzzle velocity + -14.357 * Ceramic thickness + 0.548 * Mesh size + -33.488 |

In Table 6, the mathematical equations obtained from the Linear Regression and Elastic Net algorithms are presented, each aiming to estimate the residual velocity of projectiles after impact. These equations incorporate four predictor variables: projectile type, bullet muzzle velocity, ceramic thickness, and mesh size. Each coefficient in the equations reflects the strength and direction of the relationship between the corresponding variable and the predicted residual velocity. The Elastic Net model produces a relatively balanced set of coefficients, with smaller magnitudes and both positive and negative values. This suggests a regularized model that penalizes extreme weights, reducing the risk of overfitting. Notably, the variable ceramic thickness exhibits a strong negative coefficient (−14.357), indicating its considerable inverse effect on residual velocity. The mesh size (0.548) and bullet muzzle velocity (0.554) contribute positively, while the bullet type variable (7.691) also shows a direct relationship. Conversely, the Linear Regression model yields significantly larger coefficient values, particularly for the bullet type (204.5635) and ceramic thickness (−71.9645) variables, implying higher sensitivity to those predictors. The absence of a regularization term in this method may lead to overfitting in the presence of multicollinearity or noise, especially when

dealing with relatively small datasets. From a modeling perspective, while linear regression provides a straightforward interpretation, the elastic net's use of both $L_1$ and $L_2$ regularization enables better generalization, especially when predictor variables are correlated. Therefore, in practical applications such as ballistic performance prediction, the elastic net model may offer more robust and reliable estimations.

## 4. CONCLUSION

This study has demonstrated the effectiveness of ML algorithms in predicting the residual velocity of projectiles impacting SiC ceramic armor plates, based on simulation data derived from explicit finite element analyses. By incorporating input features such as projectile type, bullet muzzle velocity, ceramic thickness, and mesh size, a predictive framework was established to estimate post-impact projectile velocity with high accuracy. Among the three algorithms evaluated, the MLP model significantly outperformed both Linear Regression and ElasticNet in terms of predictive accuracy and generalization capability. The MLP achieved an R-value of 0.9884 on the test set, with relatively low MAE and RMSE values, indicating its superior ability to model the complex, nonlinear dynamics of high-velocity ballistic impacts. In contrast, the Linear Regression model showed limited capability in capturing nonlinear patterns, while ElasticNet offered moderate improvement due to its regularization properties, though still inferior to the neural network approach. The results suggest that ML models—particularly deep learning architectures—can serve as reliable surrogates for computationally intensive numerical simulations in early-stage armor design. By enabling fast and reasonably accurate predictions, such models can support rapid evaluation of ballistic performance across different material configurations without the need for repeated physical testing or high-fidelity simulations. In addition, the study highlights the importance of data quality and diversity in training robust ML models. Although the dataset used here was derived from simulations, future research should aim to integrate experimental data for enhanced model reliability and validation. Expanding the feature space to include additional physical and geometrical parameters—such as impact angle, backing materials, and multilayer configurations—could further improve the model's predictive capability and practical relevance.

In future studies, the predictive framework developed in this work will be extended to investigate hybrid body armor systems composed of different ceramic and composite material combinations. These analyses will incorporate a variety of projectile types and employ a broader range of machine learning algorithms to evaluate residual velocity and overall ballistic performance. Such investigations are expected to provide deeper insights into material selection, optimization, and the development of more efficient and lightweight protective armor systems.

## ACKNOWLEDGMENTS

This research has received no external funding.

## AUTHOR CONTRIBUTIONS

**Halil Burak MUTU**: Methodology, Literature review, Writing, Analysis.

## CONFLICTS OF INTEREST

The author(s) has/have no competing interests to declare.

## REFERENCES

[1] A. R. Williams, The Knight and the Blast Furnace: A History of the Metallurgy of Armour in the Middle Ages & the Early Modern Period, Brill, Leiden, 2003.

[2] T. A. Otitoju, P. U. Okoye, G. Chen, Y. Li, M. O. Okoye, S. Li, "Advanced ceramic components: Materials, fabrication, and applications," Journal of Industrial and Engineering Chemistry, 85, 34-65, 2020.

[3] X. Guo, X. Sun, X. Tian, G. J. Weng, Q. D. Ouyang, L. L. Zhu, "Simulation of ballistic performance of a two-layered structure of nanostructured metal and ceramic," Composite Structures, 157, 163-173, 2016.

[4] J. Pittari III, G. Subhash, J. Zheng, V. Halls, P. Jannotti, "The rate-dependent fracture toughness of silicon carbide- and boron carbide-based ceramics," Journal of the European Ceramic Society, 35, 4411-4422, 2015.

[5] G. J. Appleby-Thomas, D. C. Wood, A. Hameed, J. Painter, B. Fitzmaurice, "On the effects of powder morphology on the post-comminution ballistic strength of ceramics," International Journal of Impact Engineering, 100, 46-55, 2017.

[6] P. Chabera, A. Boczkowska, A. Morka, P. Kędzierski, T. Niezgoda, A. Oziębło, A. Witek, "Comparison of numerical and experimental study of armour system based on alumina and silicon carbide ceramics," Bulletin of the Polish Academy of Sciences. Technical Sciences, 63, 2, 363-367, 2015.

[7] F. Cui, G. Wu, T. Ma, W. Li, "Effect of ceramic properties and depth-of-penetration test parameters on the ballistic performance of armour ceramics," Defence Science Journal, 67, 3, 2017.

[8] S. G. Savio, V. Madhu, "Ballistic performance evaluation of ceramic tiles with respect to projectile velocity against hard steel projectile using DOP test," International Journal of Impact Engineering, 113, 161-167, 2018.

[9] D. Hu, Y. Zhang, Z. Shen, Q. Cai, "Investigation on the ballistic behavior of mosaic SiC/UHMWPE composite armor systems," Ceramics International, 43, 13, 10368-10376, 2017.

[10] Z. Shen, D. Hu, G. Yang, X. Han, "Ballistic reliability study on SiC/UHMWPE composite armor against armor-piercing bullet," Composite Structures, 213, 209-219, 2019.

[11] S. Ryan, N. M. Sushma, A. K. A. V., J. Berk, T. Hashem, S. Rana, S. Venkatesh, "Machine learning for predicting the outcome of terminal ballistics events," Defence Technology, 31, 14-26, 2024.

[12] J. A. Artero-Guerrero, J. Pernas-Sánchez, J. Martín-Montal, D. Varas, J. López-Puente, "The influence of laminate stacking sequence on ballistic limit using a combined Experimental/FEM/Artificial Neural Networks (ANN) methodology," Composite Structures, 183, 299-308, 2018.

[13] Y. Wang, W. Sun, "Machine learning-based real-time velocity prediction of projectile penetration to carbon/aramid hybrid fiber laminates," Thin-Walled Structures, 197, 111600, 2024.

[14] M. Khan, M. F. Javed, N. A. Othman, S. K. U. Rehman, F. Ahmad, "Predicting penetration depth in ultra-high-performance concrete targets under ballistic impact: an interpretable machine learning approach augmented by deep generative adversarial network," Results in Engineering, 25, 103909, 2025.

[15] Z. Zhu, X. Kong, H. Zhou, C. Zheng, W. Wu, "A hybrid data-driven machine learning framework for predicting the impact resistance of composite armor," International Journal of Impact Engineering, 195, 105125, 2025.

[16] H. B. Mutu, "Machine learning-based approach for ballistic performance prediction of hybrid armors," Materials Today Communications, 113226, 2025.

[17] X. D. Lei, X. Q. Wu, Z. Zhang, K. L. Xiao, Y. W. Wang, C. G. Huang, "A machine learning model for predicting the ballistic impact resistance of unidirectional fiber-reinforced composite plate," Scientific Reports, 11, 6503, 2021.

[18] N. Kazarinov, A. Khvorov, "Predicting impact strength of perforated targets using artificial neural networks trained on FEM-generated datasets," Defence Technology, 32, 32-44, 2024.

[19] R. Andreotti, V. Leggeri, A. Casaroli, M. Quercia, C. Bettin, M. Zanella, M. V. Boniardi, "A simplified constitutive model for a SEBS gel muscle simulant-development and experimental validation for finite elements simulations of handgun and rifle ballistic impacts," Frattura e Integrità Strutturale, 16, 61, 176-197, 2022.

[20] X. Quan, R. A. Clegg, M. S. Cowler, N. K. Birnbaum, C. J. Hayhurst, "Numerical simulation of long rods impacting silicon carbide targets using JH-1 model," International Journal of Impact Engineering, 33, 1-12, 634-644, 2006.

[21] Autodyn, A.N.S.Y.S., "Theory Manual Revision 4.3," Century Dynamics, Concord, CA, 2005.

[22] T. J. Holmquist, G. R. Johnson, "Response of silicon carbide to high velocity impact," Journal of Applied Physics, 91, 9, 5858-5866, 2002.

[23] A. Araslı, "Grafen kaplı silisyum karbür seramiklerin mekanik ve balistik özelliklerinin incelenmesi," Yüksek Lisans Tezi, Fen Bilimleri Enstitüsü, [Üniversite Adı], [Şehir], Türkiye, 2022.

[24] M. Wagner, R. Adamczak, A. Porollo, J. Meller, "Linear regression models for solvent accessibility prediction in proteins," Journal of Computational Biology, 12, 355-369, 2005.

[25] J. Friedman, T. Hastie, R. Tibshirani, "Regularization paths for generalized linear models via coordinate descent," Journal of Statistical Software, 33, 1-22, 2010.

[26] H. Zou, T. Hastie, "Regularization and variable selection via the elastic net," Journal of the Royal Statistical Society B, 67, 301-320, 2005.

[27] S. Haykin, Neural Networks: A Comprehensive Foundation, Prentice Hall PTR, New Jersey, 1994.

[28] I. Goodfellow, Y. Bengio, A. Courville, Deep Learning, MIT Press, Cambridge, 2016.

[29] C. M. Bishop, N. M. Nasrabadi, Pattern Recognition and Machine Learning, Springer, New York, 2006.

[30] K. Gurney, An Introduction to Neural Networks, CRC Press, Boca Raton, 2018.

[31] Y. LeCun, Y. Bengio, G. Hinton, "Deep learning," Nature, 521, 7553, 436-444, 2015.

[32] G. P. Zhang, "Time series forecasting using a hybrid ARIMA and neural network model," Neurocomputing, 50, 159-175, 2003.

[33] H. B. Mutu, A. Özer, "Experimental and finite element analysis of ballistic properties of composite armor made of alumina, carbon and UHMWPE," Polymer Composites, 45, 15, 13844-13860, 2024.

[34] S. N. Monteiro, L. H. L. Louro, W. Trindade, C. N. Elias, C. L. Ferreira, E. de Sousa Lima, E. P. Lima Jr., "Natural curaua fiber-reinforced composites in multilayered ballistic armor," Metallurgical and Materials Transactions A, 46, 10, 4567-4577, 2015.

[35] A. Tasdemirci, G. Tunusoglu, M. Güden, "The effect of the interlayer on the ballistic performance of ceramic/composite armors: Experimental and numerical study," International Journal of Impact Engineering, 44, 1-9, 2012.

[36] P. Hu, Y. Cheng, P. Zhang, J. Liu, H. Yang, J. Chen, "A metal/UHMWPE/SiC multi-layered composite armor against ballistic impact of flat-nosed projectile," Ceramics International, 47, 16, 22497-22513, 2021.

[37] G. Crouch, G. Appleby-Thomas, P. J. Hazell, "A study of the penetration behaviour of mild-steel-cored ammunition against boron

carbide ceramic armours," International Journal of Impact Engineering, 80, 203-211, 2015.